2D parametric model for surface wave development in wind field varying in space and time

Vladimir Kudryavtsev (1,2), Maria Yurovskaya (2,1) and Bertrand Chapron (3,1)

(1) Russian State Hydrometeorological University, St. Petersburg, Russia,

(2) Marine Hydrophysical Institute, Sebastopol, Russia

(3) Laboratoire d'Oceanographie Spatiale, Ifremer, Plouzane, France,

Corresponding author:

Vladimir Kudryavtsev

e-mail: kudr@rshu.ru

Key Points

1. Fully consistent 2D parametric model of wave development under space-time varying winds is suggested.

2. 2D model is based on first-principle conservation equations consistently constrained by self-similar fetch-laws.

3. Coupled equations written in characteristic form provide practical means to rapidly assess how energy, peak frequency and direction are distributed under varying space-time wind forcing.

ABSTRACT

A fully consistent 2D parametric model of waves development under spatially and temporally varying winds is suggested. The 2D model is based on first-principle conservation equations, consistently constrained by self-similar fetch-laws. Derived coupled equations written in the characteristic form provide practical means to rapidly assess how the energy, frequency and direction of dominant surface waves are distributed under varying wind forcing. For young waves, non-linear interactions are essential to drive the peak frequency downshift, and the wind energy input and wave breaking dissipation are the governing sources of the wave energy evolution. With a prescribed wind wave growth rate, proportional to ustar/c squared, wave breaking dissipation becomes a power-function of the dominant wave slope. Under uniform wind conditions, this growth rate imposes solutions for peak frequency and energy development to follow fetch-laws, with exponents q=-1/4 p=3/4 correspondingly. This set of exponents recovers the Toba's laws, and imposes the wave breaking exponent equal to 3. A smooth transition from wind driven seas to swell is obtained. Varying wind direction is the only source to drive spectral peak direction changes. This can lead to occurrence of focusing/defocusing wave groups and formation of areas where wave-rays merge and cross. Solutions predict significant (but finite) local enhancements of the energy. Further propagating, wave rays diverge, leading to wave attenuation away from the storm area.

Plain Language Summary

A fully consistent two-dimwnsion (2D) parametric model of waves development under spatially and temporally varying winds is suggested. The 2D model is based on first-principle conservation equations, consistently constrained by empirical self-similar fetch-laws. Model equations are solved by method of characteristic. Such solutions describe evolution of wave energy, peak frequency and direction along wave-rays. This provides practical means to rapidly assess how parameters of dominant surface waves are distributed under varying wind forcing. Non-linear wave-wave interactions drive the peak frequency downshift, and the energy of the waves is governed by the balance between wind forcing and wave breaking dissipation. A smooth transition from wind driven seas to swell is obtained. Varying wind direction is the only source to drive spectral peak direction changes. This can lead to occurrence of focusing/defocusing wave groups and formation of areas where wave-rays merge and cross. Solutions predict significant (but finite) local enhancements of the energy. Further propagating, wave rays diverge, leading to wave attenuation away from the storm area. Suggested model is further applied to simulate the surface waves generated by Tropical Cyclones

1. Introduction

An efficient and ready-to-use statistical description of the surface gravity wave field, especially its directional energy characteristics, is often needed for many engineering and scientific applications, in particular, for short-term forecasting of surface waves generated by Tropical Cyclones (TC). Full sophisticated spectral wave models certainly have the capability to provide detailed wave information. As an example, Moon et al. [2003] performed a comprehensive investigation of wind wave field generated by TC Bonnie using WAVEWATCH III model [Tolman, 2009], buoy and aircraft Scanning Radar Altimeter (SRA) measurements. This study clearly demonstrated that using realistic wind forcing, the use of a high-resolution WAVEWATCH III model may yield successful simulations of surface wave fields in hurricane conditions.

Yet, computer limitations and/or needs to consider ensembles of solutions also invite to develop more simplified solutions. For instance, practical models can help to rapidly anticipate and document the role of partial resonance effects to increase the effective fetch and duration of the wave-growth process in the main direction of the tropical and extra-tropical weather systems, i.e. the wave trapping phenomenon [e.g., King and Shemdin, 1978; Dysthe and Harbitz, 1987; Young, 1988; Bowyer and MacAfee, 2005; Young and Vinoth, 2013; Kudryavtsev et al., 2015]. Indeed, despite the spatio-temporal complexity of extreme weather systems, generated surface waves are generally found to well follow self-similar fetch laws, originally suggested by Kitaigorodskii [1962]. For very intense low pressure systems, the main vortex structure of the winds apparently solely governs the spatial distribution of the waves and their associated directional characteristics. In that context, Wright et al. [2001] and more recently, Hwang and Fan [2017], Hwang and Walsh [2018], analyzed and quantified the azimuthal and radial distributions of wave spectra measured by airborne scanning radar altimeter inside tropical cyclones. While the front half of the cyclone is well characterized by single wave systems, multiple wave systems are generally observed in the back and right quarters outside the radius of maximum wind. Hwang and Fan [2017], Hwang and Walsh [2018] further suggested an empirical model to describe the equivalent fetch and the dominant wave propagation direction.

More generally, for waves generated by varying wind field in both space and time, parametric models [e.g. Hasselmann et al., 1976; Gunther et al., 1979] should be more relevant. The parametric models simplify the evolution of the wave spectrum parameters: energy (significant wave height), frequency of the peak and its direction. The equations describing the evolution of relevant spectral moments are derived from the kinetic energy and momentum equations.

Suggested by Hasselmann et al. [1976], the main principle of the parametric model construction is that the energy and momentum source terms can be specified to reproduce empirical fetch laws for idealized cases (i.e., constant wind forcing condition).

In this paper, the main objective is to revise and pursue this heuristic approach, to propose the derivation of practical and fully consistent solutions for surface wave developments under spatially and temporally varying winds. Starting from first-principle governing equations, section 2, consistently constrained by self-similar fetch-laws, section 3, a final set of coupled equations is then finally obtained, section 4, to describe the energy and directional evolution of the dominant peak waves along their propagation characteristics. Illustrative model exemplars are discussed, section 5. Conclusions follow, section 6. More results of this model to wave field developments under moving Tropical Cyclones (TCs) are given in a following companion paper.

2. Governing Equations

The parametric model considered here is limited to three main spectral parameters: energy, e, spectral peak frequency, ω_p, and its main direction φ_p, which are derivatives of the 0th – and the 1st –moments of the wave spectrum. Equations of conservation for the spectral density of the energy, $E(\omega,\varphi)$, and momentum, $M_i(\omega,\varphi)$ are [Hasselmann et al., 1976; Phillips, 1977]:

$$\partial E / \partial t + c_{gj}\partial E / \partial x_j = S^E \qquad (1a)$$

$$\partial M_i / \partial t + c_{gj}\partial M_i / \partial x_j = S_i^M \qquad (1b)$$

where c_{gj} is the group velocity, S^E and S_i^M the energy and momentum sources. The directional spectrum is represented as $E(\omega,\varphi) = A(\varphi-\varphi_p)F(\omega)$, where $A(\varphi-\varphi_p)$ the angular spreading, function satisfying condition $\int A d\varphi = 1$, and $F(\omega)$ is omnidirectional frequency spectrum. In the gravity range, the momentum spectrum $M_i(\omega,\varphi)$ is related to $E(\omega,\varphi)$ as: $M_i = k_i E/\omega = \kappa_i \omega E/g$ where κ_i is the unit wavenumber vector: $\kappa_i = [\cos\varphi, \sin\varphi]$. Correspondingly, the energy and the momentum total sources are linked as:

$$S_i^M = \kappa_i \omega S^E / g \,. \qquad (2)$$

The energy source S^E is usually represented as the sum of the energy input from the wind (wind forcing), S_W, wave breaking dissipation, S_D, and the non-linear four-wave interactions, S_N: $S^E = S_W - S_D + S_N$.

Wind forcing can generally be defined within the frame of the quasi-linear theory of wave generation as

$$S_W = \beta \omega A(\varphi - \varphi_p) F(\omega), \qquad (3a)$$

where β is a growth rate specified here as [e.g. Plant, 1982]

$$\beta = c_\beta \left(u_* / c\right)^2 \cos^2(\varphi - \varphi_W) \qquad (3b)$$

with $c_\beta = 4 \times 10^{-2}$, u_* the air friction velocity, and φ_W the wind direction. Relationship (3b) is only valid for waves traveling slower than the projection of the wind velocity on their directions. For $u_k \cos(\varphi - \varphi_W) - c < 0$, with u_k the wind speed at the height $z = k^{-1}$, the growth rate becomes negative, $\beta < 0$, i.e. the wind input becomes an energy sink [see e.g. Merlink et al., 2000, and references cited therein]. In the present study, we ignore negative values of β replacing them by zero, as:

$$\beta = c_\beta \left(u_* / c\right)^2 \cos^2(\varphi - \varphi_W) H_\beta(\varphi - \varphi_W, u_{10}/c) \qquad (3c)$$

where H_β is a step-like (Heaviside type) function,

$$H_\beta(\varphi - \varphi_W, u_{10}/c) = \frac{1}{2}\left[1 + \tanh\left(p\left(\cos(\varphi - \varphi_W)\frac{u_{10}}{c} - 0.85\right)\right)\right] \qquad (3d)$$

with p is a large number assigned here as p =30. For sake of simplicity, we replace u_k in (3b) by u_{10}.

Expression for the nonlinear interaction term S_N can be derived from first principles [Hasselmann, 1962; Zakharov, 2010]. Exact calculations of S_N may be time consuming, and approximate schemes have been proposed [e.g. discrete interaction approximation (DIA), Hasselmann et al. 1985; or its extension, - the multiple DIA, Tolman 2004]. Finally, a precise expression for the dissipation term is not known and different phenomenological approximations [e.g. model of dissipation due to wave capping by Hasselmann, 1974] are usually adopted for the wave development simulations.

However, a proper determination of the energy source, solution of the energy and momentum conservation equations must reproduce general semi-empirical properties of wave development expressed through the fetch-limited laws and shape of the wave spectrum. This is the general principle of the parametric model construction. Following this approach suggested by Hasselmann et al. [1976], the fetch-limited laws can indeed determine and constrain the energy and momentum source terms.

2.1. Energy

Integral of (2.1a) over all frequencies and directions provides the total energy, $e = \iint E d\varphi d\omega$, and the conservation equation writes:

$$\begin{aligned} \partial e / \partial t + \kappa_j^p \overline{c}_g \partial e / \partial x_j + e \partial (\kappa_j^p \overline{c}_g) / \partial x_j &= \iint S^E d\varphi d\omega \\ &\approx \iint (S_W - S_D) d\varphi d\omega \end{aligned} \tag{4}$$

where $\overline{c}_g$ is the mean group velocity weighted over the entire spectrum

$$\overline{c}_g = \int c_g F(\omega) d\omega \Big/ e , \tag{5}$$

and κ_j^p is unit vector of the spectral peak direction:

$$\kappa_j^p = [\cos\varphi_p, \sin\varphi_p]. \tag{6}$$

For the JONSWAP spectrum [Hasselmann et al., 1980], $\overline{c}_g$ can be evaluated, $\overline{c}_g = r_g c_{gp}$, with $r_g \simeq 0.9$, where c_{gp} is the group velocity of the spectral peak. After integration over ω and φ, contributions associated to source S_N cancel out, and the total energy is mainly governed by wind energy input and dissipation. This statement should not lead to the erroneous conclusion on a negligible role of non-linear four-wave interactions for the wave energy evolution. Non-linear interactions are essential. Non-linear interactions implicitly appear to control the peak frequency downshift of the energy-containing part of the spectrum, subject to wind forcing and wave breaking dissipation (see below for more discussion).

2.2. Spectral Peak Kinematic

To describe the evolution of the spectral peak frequency and its direction, the momentum conservation equations are to be used [Gunther et al., 1981].

2.2.1. Frequency

Multiplying (1b) by κ_i and integrating the resulting equation over ω and φ, it follows

$$\frac{\partial}{\partial t}\left(\overline{\omega} e\right) + \frac{\partial}{\partial x_j}\left(\kappa_j^p \overline{c}_g \overline{\omega} e\right) = g \iint \kappa_i S_i^M d\varphi d\omega \qquad (7)$$

where $\overline{\omega}$ is the mean frequency weighted over the spectrum

$$\overline{\omega} = \int \omega F(\omega) d\omega \Big/ e \qquad (8)$$

For the JONSWAP spectrum, $\overline{\omega}$ is related to the spectral peak frequency, ω_p, as $\overline{\omega} \approx 1.15\omega_p$. The ratio $\omega_p / \overline{\omega}$ is close to $\overline{c}_g / c_{gp} = r_g$, (about 5% difference), and for the sake of simplicity, we consider $\omega_p / \overline{\omega} = \overline{c}_g / c_{gp} = r_g$. This is already applied in (2.6), where we replaced $(g/2\overline{\omega})$ by $\overline{c}_g$.

Eq. (7), with use of (4), leads to the following equation for the evolution of the peak frequency, ω_p:

$$\frac{\partial}{\partial t}\omega_p + \kappa_j^p \overline{c}_g \frac{\partial}{\partial x_j}\omega_p = \frac{r_g}{e}\int(\omega - \overline{\omega})S_O^E d\omega \qquad (9)$$

where $S_O^E(\omega) = \int S^E(\omega,\varphi)d\varphi$ represent the omnidirectional energy source. Expanding S_O^E into Taylor series $S_O^E(\omega) = S_O^E(\overline{\omega}) + \left(\partial S_O^E/\partial\omega\right)(\omega - \overline{\omega}) + ...$ the evolution of the peak frequency is thus governed by the derivative of S_O^E over ω in the vicinity of the spectral peak, i.e. $\propto (\delta\omega)^2\,\partial S_O^E/\partial\omega$, where $(\delta\omega)^2$ relates to the spectral spread in the frequency domain. Since, under growing sea conditions, both wind forcing, S_W, and dissipation, S_D, have local extrema (maximum and minimum, correspondingly) in the peak vicinity, $\omega = \overline{\omega}$, the main mechanism leading to spectral peak downshifts is thus S_N. Indeed, S_N exhibits a strong spectral gradient in this peak spectral area [see e.g. Fig.4b in Hasselmann et al., 1976 for illustration]. Under growing sea conditions, the balance of wind forcing and dissipation provides energy gain to the dominant waves, see Eq. (4), but downshifts of their frequency peaks are driven by non-linear four-wave interactions which redistribute the energy between wave components.

However, when developing waves approach the fully developed conditions, i.e. when the inverse wave age, $\alpha = u_{10}/c_p$, is $\alpha \to 0.85$, wind energy input (3d) is decreasing. Around the peak, the gradient of the total source, $\partial S_O^E/\partial\omega$, becomes more strongly affected by this wind-energy-input decay. The gradient of S_W is positive, in contrast to S_N, and acts to restrain the spectral peak downshift when waves are approaching a fully developed stage.

2.2.2. Direction

For the evolution of the spectral peak direction, the momentum equation (1b) is first integrated over ω and φ, leading to

$$\frac{\partial}{\partial t}\left(\kappa_i^p \overline{\omega} e\right) + \frac{\partial}{\partial x_j}\left(\kappa_i^p \kappa_j^p \overline{c}_g \overline{\omega} e\right) = g\iint S_i^M d\varphi d\omega \qquad (10)$$

Then, using (7) and (2), we have

$$\frac{\partial}{\partial t}\varphi_p + \kappa_j^p \overline{c}_g \frac{\partial}{\partial x_j}\varphi_p = \frac{1}{\overline{\omega} e}\iint \sin(\varphi - \varphi_p)\omega S^E d\varphi d\omega \qquad (11)$$

Source terms associated to dissipation, S_D, and non-linear four-wave interactions, S_N, are functions (or functional) of the wave spectrum. Therefore, S_D and S_N peak directions should also coincide with the spectral peak direction, φ_p. The azimuthal integration for S_D and S_N thus vanishes. Hence, changes of the peak wave direction are mostly impacted by veering wind conditions.

The directional spreading of wave energy, $A(\varphi - \varphi_p)$, is further assumed to be much narrower than the angular distribution of the wind energy source term (3c). Then, substituting (3c) into the r.h.s. of (11) and expanding φ-dependent functions into Taylor series around $\varphi = \varphi_p$ up to the second order, we obtain the following:

$$\frac{\partial}{\partial t}\varphi_p + \kappa_j^p \overline{c}_g \frac{\partial}{\partial x_j}\varphi_p = -C_\varphi \alpha^2 \omega_p H_p \sin\left[2(\varphi_p - \varphi_W)\right] \qquad (12)$$

where H_p is the step-like function (3d) applied for the spectral peak parameters, and C_φ relates to spectral moments :

$$C_\varphi = c_D c_\beta \delta\varphi^2 \frac{\int \omega^4 F(\omega) d\omega}{\omega_p^3 \int \omega F(\omega) d\omega} \qquad (13)$$

where c_D is the drag coefficient, and $\delta\varphi^2$ corresponds to the angular spread of wave energy: $\delta\varphi^2 = \int (\varphi - \varphi_p)^2 A(\varphi - \varphi_p) d\varphi$, equal to $\delta\varphi^2 = 0.16$ for the JONSWAP-type spectrum. To note, in (13), the integral in numerator of the fraction can be divergent, if all wave spectral components are integrated (with the upper limit as $\propto \ln\omega$). Therefore, to evaluate C_φ, it can be

suggested to restrict the spectral domain integration to $\bar{\omega} - \delta\omega < \omega < \bar{\omega} + \delta\omega$. Numerically evaluated using the JONSWAP spectrum, the fraction in (13) is about 1.4.

Equation (12) can be compared with previously suggested semi-empirical relations [Gunther et al., 1981; Vledder and Holthuijsen, 1993 and references cited therein]. The r.h.s. of (12) can be interpreted as a wave directional relaxation approximation: $-\sin(\varphi_p - \varphi_w)/T_R$, where T_R is a relaxation time-scale evaluated semi-empirically as:

$$1/T_R = c_r (g/u)\alpha^r \qquad (14)$$

where r is an exponent, and c_r is an empirical constant. For $r = 2$, c_r is reported to vary from $c_r = 5.3\times10^{-5}$ to $c_r = 1.4\times10^{-4}$, and for $r = 1$, c_r varies from $c_r = 6\times10^{-5}$ to $c_r = 1.2\times10^{-4}$ [see Table 3 from Vledder and Holthuijsen, 1993, and references cited therein for r and c_r]. Under our proposed development, Eq. (12), the relaxation approximation leads to $1/T_R = 2C_\varphi (g/u)\alpha^3$, where the factor 2 takes into account the angle change in the sinus function in (12). The dependency of T_R on wave age is also stronger than experimentally reported, power exponent 3 against 2 or 1. But the model proportionality coefficient equals to $2C_\varphi = 3.6\times10^{-5}$ (at $c_\beta = 4\times10^{-2}$ and $c_D = 2\times10^{-3}$), consistent with reported empirical parameters in the range of wave age $\alpha = 1 \div 3$.

3. Input sources: Link to self-similarity

Except for the wave direction, Eq. (12), the source terms for the conservation equations for the energy (4) and frequency (9) are not defined. Following Hasselmann et al. [1976], fetch-limited laws can be used to "calibrate" these source terms, i.e. to reproduce wind-wave development characteristics for stationary wind conditions [see e.g. review in Badulin at al., 2007]:

$$\tilde{\omega}_p \equiv \alpha = c_\alpha \tilde{x}^q, \quad \tilde{e} = c_e \tilde{x}^p \qquad (15a)$$

where $\tilde{x} = xg/u^2$ is the dimensionless fetch, u is the wind speed (e.g. wind speed at 10 meter height), g is the gravity acceleration, $\tilde{\omega}_p = \omega_p u/g$ and $\tilde{e} = eg^2/u^4$ are dimensionless spectral peak frequency and energy. These self-similar laws (15a) can be represented as one-parametric expression to linking the dimensionless energy and the wave age

$$\tilde{e} = c_e \left(\alpha / c_\alpha\right)^{p/q} \tag{15b}$$

3.1. Energy

The input energy source in Eq. (4) is defined as

$$\iint \left(S_W - S_D\right) d\varphi d\omega = I_w - D \tag{16}$$

where I_W is the integral wind energy input which using (3c) is

$$I_W = r_W c_\beta \left(u_* / c_p\right)^2 \cos^2(\varphi_p - \varphi_W) H_p \omega_p e \tag{17}$$

with $r_W = \int \omega^3 F d\omega \Big/ (\omega_p^3 e)$, evaluated to r_W = 2.35, for a JONSWAP spectrum. The integral dissipation D in (16) is expressed by considering a non-linear attenuation based on a threshold steepness criterion:

$$D = \omega_p e \left(k_p^2 e / \varepsilon_T^2\right)^n \tag{18}$$

where k_p is the spectral peak wavenumber, ε_T^2 is a threshold steepness, n defines the non-linear attenuation. For fetch-limited and uniform wind conditions, we can suggest the integral dissipation to be proportional to the integral wind input, i.e. $D/I_w = \gamma$ where $\gamma < 1$ is a constant. Integral dissipation and inverse wave age are then linked : $\left(k_p^2 e\right)^n \propto \alpha^2$. Using fetch-laws (15), the dissipation exponent can then be defined from the exponents of the fetch laws:

$$n = \frac{2q}{p + 4q} \tag{19}$$

For the case of fetch-wave development, Eq. (4) then becomes:

$$\partial(\overline{c}_g e)/\partial x = r_W c_\beta c_D (1-\gamma)\left(g/u\right)\alpha^3 e \tag{20}$$

and reorganized using fetch-laws (15) as

$$\begin{aligned}\partial \ln(e/\alpha)/\partial\tilde{x} &= 2b\alpha^4 \\ &= 2bc_\alpha^4 \tilde{x}^{4q}\end{aligned} \tag{21}$$

with $b = (r_W/r_g)(1-\gamma)c_\beta c_D$. Equation (21) will provide fetch-law-type solutions, only if the fetch law exponent q in the r.h.s. of (21) equals to

$$q = -1/4 \tag{22}$$

Notice, that this value is linked to the wind input source term (17), where $\beta \propto \left(u_*/c_p\right)^2$. Adopting another parametrization for the growth rate in (3b), e.g. $\beta \propto u_*/c_p$ [Snyder et al., 1981] or $\beta \propto \left(u_*/c_p\right)^{4/3}$ [Pushkarev and Zakharov, 2015], the exponent of α in the r.h.s. of (21) becomes "3" or "10/3", leading to the fetch-law exponents $q = -1/3$ or $q = -0.3$, correspondingly. These values are certainly acceptable, and have been used in previous parametric models [Hasselmann et al., 1976; Fontaine, 2013].

Keeping $q = -1/4$, i.e. growth rate Eq.(3b), the constant b in Eq. (21) is also linked to the fetch-law parameters as

$$b = \frac{1}{2}(p-q)c_\alpha^{-4} \tag{23}$$

Given r_W, r_g, c_β, c_D, the proportionality constant γ can then be derived :

$$(1-\gamma) = (p-q)c_\alpha^4/(2c_\beta c_D\, r_W/r_g)\,. \tag{24}$$

Subsequently, the threshold steepness, ε_T^2, is deduced from $\gamma = \left(k_p^2 e/\varepsilon_T^2\right)^n \Big/ \left[\alpha^2\left(c_\beta c_D\, r_W/r_g\right)\right]$, and using (15b), expressed as

$$\varepsilon_T^2 = \frac{c_e c_\alpha^{-p/q}}{\left(\gamma c_\beta c_D \, r_W / r_g\right)^{1/n}} \tag{25}$$

The integral source term, $I_w - D$, in the energy conservation equation (4), calibrated on fetch-law constants, finally reads:

$$\begin{aligned} I_w - D &= \omega_p e\left(\tilde{I}_w - \tilde{D}\right) \\ \tilde{I}_w - \tilde{D} &= C_e H_p \alpha^2 \cos^2(\varphi_p - \varphi_W) - \left(e k_p^2 / \varepsilon_T^2\right)^n \end{aligned} \tag{26}$$

with C_e absorbing other constants $C_e = 1/2 \times (p-q)/(1-\gamma) c_\alpha^{-4}$, and ε_T^2 and γ given by (24) and (25). To note, when $\alpha \cos(\varphi_p - \varphi_W) < 0.85$ is locally fulfilled, the wind energy input is switched off, and waves turn into regime of swell and attenuate under dissipation.

3.2. Peak frequency

3.2.1. Effect of non-linear interactions

As discussed in sec 2.2.1, during the active stage of wave development, the waves are young, and non-linear four-wave interactions control the peak frequency downshift. In the frequency conservation equation (9), the input source term can be estimated as

$$\begin{aligned} e^{-1} \int (\omega - \overline{\omega}) S_O^N d\omega \approx & \\ & \approx e^{-1} \partial S_O^N / \partial \omega \int (\omega - \overline{\omega})^2 d\omega \\ & \propto -e^{-1} \delta\omega^2 \left\langle S_O^N \right\rangle \\ & \propto -\omega_p^2 k_p^4 e^2 \propto -g^{-4} \omega_p^{10} e^2 \end{aligned} \tag{27}$$

where $\delta\omega \propto \omega_p$ is a spectral frequency width. Taking into account $\left\langle S_O^N \right\rangle$ is cubic with wave energy, the derivative of S_O^N over ω is negative with a minimum around the spectral peak, and evaluated as $\partial S_O^N / \partial \omega \propto \left\langle S_O^N \right\rangle / \delta\omega$ [e.g. Zakharov, 2010; Badulin et al., 2007]. Eq. (9) with (27) for fetch-limited conditions then reads

$$c_{gp} \partial \omega_p / \partial x \propto -g^{-4} \omega_p^{10} e^2 \tag{28}$$

Substituting parameters derived from fetch-laws (15), the so-called “magic” universal relationship between fetch-law exponents is recovered [Badulin et al., 2007; Zakharov, 2010]:

$$2p + 10q + 1 = 0 \tag{29}$$

Since q is already prescribed, $q = -1/4$ (to satisfy the energy balance equation), the relationship (29) dictates the exponent for the energy equal to

$$p = 3/4 \tag{30}$$

This set of exponents, $q = -1/4$ and $p = 3/4$, corresponds to fetch laws suggested by Toba [1972]. These exponents further determine the exponent n for the wave breaking dissipation (18), and according to (19) it becomes $n = 2$.

Substituting (15) in (28), the proportionality constant in (28) is derived, leading to:

$$\begin{aligned} e^{-1}\int(\omega - \bar{\omega})S_O^N d\omega &= C_\alpha g^{-4}\omega_p^{10}e^2 \\ &= C_\alpha \omega_p^2 \left(k_p^2 e\right)^2 \end{aligned} \tag{31}$$

with C_α absorbing the fetch law parameters: $C_\alpha = 1/2 \times q c_\alpha^{-10} c_e^{-2}$, and the downshift of the spectral peak frequency is proportional to the wave energy to power 2 (or proportional to the slope of the spectral peak waves to power 4).

While non-linear four-wave interactions are governing this peak frequency downshift, an alternative view can also be hypothesized. In random rough seas, the dominant waves occur in groups. At the centers of these groups, waves can exceed a critical steepness leading to breaking events. Suggested by Tulin [1996], breaking events can then contribute to local spectral peak downshifts [see also Fontaine, 2013 for more references and discussion]. According to Tulin [1996], the peak downshift rate is proportional to D/e. In the present development $D/e \propto \left(k_p^2 e\right)^2$, and Eq. (31) is consistent with Tulin’s hypothesis. Though the underlying physics is different, four-wave interactions or wave breaking dissipation, wave group occurrence link

these processes. Indeed, Longuet-Higgins [1976] pointed out that most of the non-linear energy transfer occurs among groups. This can explain the resulting Eq.(31) governing the spectral peak downshift to be formally equivalent for both processes.

3.2.2. Effect of wind input

As already discussed in sec.2.2.1, the non-linear interactions govern the peak frequency downshift as long as the waves are young. When waves approach the fully developed conditions, $\alpha\cos(\varphi_p-\varphi_W)\to 0.85$, the wind energy input (3c) with (3d) rapidly decays, to impact the gradient of the energy source around the peak, $\partial S_O^E/\partial\omega$, and thus, according to (9), the peak frequency downshift. The rate of peak downshift associated to the wind forcing writes

$$\partial\omega_p/\partial t = e^{-1}\int\int_{\bar{\omega}-\delta\omega}^{\bar{\omega}-\delta\omega}(\omega-\bar{\omega})S_O^W d\omega \qquad (32)$$

with S_O^W the omnidirectional wind source term. This rate is shown in Fig.1 along with the downshift rate due to four-wave interactions (31). For young sea, the wind forcing weakly contributes to peak downshift of young waves. For waves approaching full development, $\alpha\to 0.85$, the wind forcing starts to significantly act against the downshift driven by non-linear four-wave interactions. Near $\alpha\approx 0.85$, the magnitudes of non-linear and wind induced downshift rates are comparable, but with opposite signs. This leads to decelerate the peak downshift, leveling off the peak frequency.

For $\alpha<0.85$, the wind forcing could lead to “upshift” the spectral peak. The wind energy input vanishes in the vicinity of the spectral peak, and taking into account the attenuation due to dissipation, the spectral peak shape can be deformed and shift towards higher frequencies, more subject to wind forcing.

Figure 1 is about here

To take this effect into account, a bell-shaped function,

$$\Delta_p = 1\text{-}1.25 \times \mathrm{sech}^2\left[10(\alpha_p - 0.9)\right],$$

simulating right plot in Fig.1 (with $\alpha_p = \cos(\varphi_p - \varphi_W)\, u_{10}/c_p$), is introduced in Eq. (31) to largely reduce the peak downshift if the phase velocity approaches the wind velocity, and to upshift the peak frequency if the wind energy input locally vanishes. This function corresponds to the derivative of the step-like function (13), used to limit the wind energy input for fully developed waves. The r.h.s. of the peak frequency conservation equation (9) finally writes:

$$e^{-1}\int(\omega - \bar{\omega})S_O^E d\omega = r_g C_\alpha \Delta_p \omega_p^2 \left(k_p^2 e\right)^2 \tag{33}$$

4. Model Equations: ray characteristic form

Equations (4) with (26) can be expressed in ray characteristic form as:

$$\frac{de}{dt} = -e\left(\partial\bar{c}_g/\partial l + \bar{c}_g\, \partial\varphi_p/\partial n\right) + \omega_p e\left(\tilde{I}_w - \tilde{D}\right) \tag{34}$$

where $d/dt = \partial/\partial t + \kappa_j^p \bar{c}_g\, \partial/\partial x_j$ is the total derivative for wave train traveling along the ray

$$\frac{d}{dt}x_j = \kappa_j^p \bar{c}_g \tag{35}$$

where we remind that $\bar{c}_g$ is the mean group velocity linked the group velocity of the spectral peak as $\bar{c}_g = r_g c_{gp}$.

4.1. Effect of group velocities divergence

The first term in the r.h.s of (34) corresponds to the divergence of the group velocity, $\partial(\kappa_j^p \bar{c}_g)/\partial x_j$, written in local orthogonal coordinates, where l and n are directed along and normal to the ray trajectory, correspondingly. Along-ray and cross-ray components of the group velocity divergence are

$$\partial\bar{c}_g/\partial l \approx \Delta\bar{c}_g/(\bar{c}_g\Delta t) = \bar{c}_g^{-1}\, d\bar{c}_g/dt \tag{36}$$

$$\overline{c}_g \, \partial\varphi_p / \partial n \simeq \overline{c}_g \, \Delta\varphi_p / \Delta n \,, \tag{37}$$

where $\Delta\varphi_p$ is the difference between neighbor characteristics separated by the small distance Δn, evolving in time as

$$d\Delta n / dt = \Delta\varphi_p \overline{c}_g \tag{38}$$

Equation for $\Delta\varphi_p$ follows

$$\frac{d}{dt}\Delta\varphi_p = -T^{-1}\left[\left(\Delta\varphi_p - \Delta\varphi_w\right) + \frac{\Delta u}{u}\tan\left(2(\varphi_p - \varphi_W)\right)\right] \tag{39}$$

with T is a relaxation time scale defined as

$$T^{-1} = 2C_\varphi H_p \alpha^2 \omega_p \cos\left(2(\varphi_p - \varphi_W)\right), \tag{40}$$

$\Delta\varphi_W$ and Δu are the wind direction and speed differences between neighbor characteristics. Developing young seas are almost align with the wind, $\varphi_p \approx \varphi_w$. Then ignoring the impact of wind speed difference, second term in the square brackets of r.h.s of (19), we obtain

$$\begin{aligned} \frac{d}{dt}\Delta\varphi_p + T^{-1}\Delta\varphi_p &= T^{-1}\Delta\varphi_w \\ &= T^{-1} G_W^n \Delta n \end{aligned} \tag{41}$$

where $G_W^n = \Delta\varphi_w / \Delta n$ is the cross-ray component of the wind direction gradient. Solution of the coupled system, (38) and (41), can further be combined.

Defining the cross-ray gradient of wave direction, $G_n = \Delta\varphi_p / \Delta n$, which takes into account the cross-ray divergence of group velocities, the energy balance (34) now becomes:

$$\frac{d}{dt}\ln(\overline{c}_g e) = -\overline{c}_g G_n + \omega_p\left(\tilde{I}_w - \tilde{D}\right) \tag{42}$$

Note, the coupled (38) and (41) can also be combined to describe the evolutions of the cross-ray gradient:

$$dG_n/dt + G_n/T + \overline{c}_g G_n^2 = G_W^n/T \tag{43}$$

4.2. Caustic formation

Integrating (38), the distance between neighbor characteristics, Δn , evolves in time as

$$\Delta n = \Delta n_0 + \int_{t_0}^{t} \overline{c}_g \Delta\varphi_p dt \tag{44}$$

where Δn_0 is an initial distance. If ray paths converge, i.e. $\Delta\varphi_p < 0$, Δn may vanish at some location. The term $G_n = \Delta\varphi_p/\Delta n$ tends to infinity, and Eq. (42) loses its validity. This phenomenon corresponds to the formation of a "caustic point". In this development, such a singularity is a direct consequence of the assumption that a wave group is almost monochromatic. In nature, wave trains have a finite spectral band-width. It leads to group velocity variations, with a standard deviation, Δc_g , defined as

$$\left(\Delta c_g\right)^2 = \int_{t_0}^{t} \left(c - \overline{c}_g\right)^2 F(\omega) d\omega \tag{45}$$

For the JONSWAP spectrum, Δc_g scaled by the mean group velocity is $\left(\Delta c_g/\overline{c}_g\right)^2 = 4.6\times10^{-2}$. Dominant waves can then be represented by a superposition of elementary monochromatic beams. At a given time, positions of elementary waves, as well as their contribution to the total cross-ray divergence, are distributed along the ray, around the mean position $l = \overline{c}_g t$ and within the interval $\Delta l / l = \pm\Delta c_g / \overline{c}_g$. The overall impact of these superposed wave beams on the mean cross-ray group velocity divergence is discussed in the Appendix. For the cross-ray gradient of the waves directions, $G_n = \Delta\varphi_p/\Delta n$, the averaged contribution of these elementary waves reads

$$G_n = \frac{\Delta\varphi_p}{\Delta n_0}\left[\frac{\Delta n/\Delta n_0}{\left(\Delta n/\Delta n_0\right)^2 + \left(1/2\cdot\Delta c_g/\overline{c}_g\right)^2}\right] \tag{46}$$

where $\Delta\varphi_p$ and Δn are solutions of the equations system (41) and (38).

4.3. Final Set of model equations

Assembling the different equations written in the characteristic form, the final closed system of differential equations becomes:

$$\frac{d}{dt}\ln(\overline{c}_g e) = -\overline{c}_g G_n + \omega_p \left(\tilde{I}_w - \tilde{D}\right) \tag{47}$$

$$\frac{d}{dt} c_{gp} = -\frac{r_g C_\alpha}{2} \Delta_p g \left(k_p^2 e\right)^2 \tag{48}$$

$$\frac{d}{dt}\varphi_p = C_\varphi \alpha^2 \omega_p H_p \sin\left[2(\varphi_p - \varphi_W)\right] \tag{49}$$

$$\frac{d}{dt} x_j = \kappa_j^p \overline{c}_g \tag{50}$$

where the cross-ray divergence factor G_n, and dimensionless rate of wind input-minus-dissipation $\tilde{I}_w - \tilde{D}$ in (4.47) are defined by (46) and (26) correspondingly; the peak frequency conservation equation (48) is expressed in terms of the spectral peak group velocity, $c_{gp} = g/(2\omega_p)$. The mean group velocity appearing in (47) and (50) is linked to c_{gp} as: $\overline{c}_g = r_g c_{gp}$. A summary of the model constants is given in Appendix 2.

As established, this coupled system describes the development of surface waves under a varying wind field in both space and time, as well as the evolution of swell propagation when the wind forcing is switched off.

This system can further be supplemented with a relationship describing the breaking of the dominant waves. In terms of the total length of breaking crests, L, the energy dissipation is [Phillips, 1985]

$$D = b g^{-1} c^5 L \tag{51}$$

with b in the range $b = 10^{-4} \div 10^{-2}$. In the present model development, the dissipation is defined by (18), leading to the following relation for the length of breaking crests of dominant waves:

$$L_p = b^{-1}\varepsilon_T^2 k_p \left(ek_p^2/\varepsilon_T^2\right)^3 \quad (52)$$

Correspondingly, the fraction of sea surface covered by peak wave breakers, the whitecap coverage, $Q_p = \varepsilon k_p^{-1} L_p$, with $\varepsilon \ll 1$, can be evaluated

$$Q_p = c_Q \left(ek_p^2/\varepsilon_T^2\right)^3 \quad (53)$$

where $c_Q = b^{-1}\varepsilon_T^2\varepsilon$ is absorbing the other constants. Whitecap coverage is proportional to the peak wave steepness to power "6". For developing waves, $ek_p^2 \propto \alpha$ and $Q_p \propto \alpha^3$, hence the younger the waves the larger is the fraction of the surface covered by whitecaps. If the peak frequency is fixed, the whitecaps coverage becomes proportional to the wind speed to power "3", as often reported [see e.g. Brumer et al., 2017, and references cited therein]. If the fetch is fixed, $\alpha \propto \left(xg/u^2\right)^{-1/4}$), the whitecap coverage is proportional to the wind speed to power "3/2".

Note, breakers from the equilibrium range of wind waves likely provide the major part of the whitecap coverage, Q_e, which is least dependent (if dependent at all) on wave age and mostly driven by the wind [Phillips, 1985]. The total whitecap coverage thus corresponds to the sum $Q = Q_p + Q_e$, and this spatial distribution is both wind speed and wave-age dependent. Yet, the largest thickness of foam layers is more likely associated with dominant wave breakers [Reul and Chapron, 2003]. Emitted radiations from thick foam-induced brightness temperature will generally rise and impact low-frequency microwave measurements, especially under extreme conditions [e.g. Reul et al., 2017]. For these intense and varying wind conditions, the distributed thickness of foam layers is then expected to be strongly wave-age dependent.

5. Model exemplars

5.1. Uniform wind: recovering fetch laws

An example of the model performance for a fetch-limited wave development is shown Fig.2. For reference, the empirical dependencies of the dimensionless energy and wave age on fetch suggested by Babanin and Soloviev [1998] are also shown. At early stage of development, the model reproduces these empirical dependencies, in accord with the definition of the model input source terms calibrated on fetch-laws. More importantly, the model provides a smooth transition from developing to fully developed waves. This corresponds to the decay of the wind energy input that restrains both the energy growth and the peak frequency downshift.

When the wind forcing is switched off at dimensionless fetch $\tilde{x} = 8 \times 10^4$, Fig.2, the energy balance is suddenly lost at this fetch, leading to a rapid decay of the wave energy and a moderate downshift of the peak frequency. At this stage, the restraining action associated to the spectral gradient of the wind forcing vanishes, and the downshift results from the energy transfer associated to non-linear wave interactions. Strongly dependent on the wave steepness, the significant decrease of the dominant wave energy then contributes to level off the peak downshift.

Following the present development, it is worth to note that the evolution of the swell system is also self-similar, i.e. the evolution is described by the same dimensionless functions of dimensionless space and time variables. The rate of swell energy attenuation is then found much larger than predicted by Zakharov and Badulin [2017] under the weakly turbulent theory, which predicts an energy decrease as $\propto x^{-1/12}$.

Figure 2 is about here

5.2. Wind velocity divergence/convergence effects

Next, we consider the case of a fetch-limited wave development under the action of a wind, uniform in the main direction, but varying in the perpendicular direction. As a prototype, a roll-like structure of the wind field is suggested: the wind velocity component of the main flow, u_{10}, is constant, and the orthogonal component, v, only varies in the y-direction. It is also assumed

that $v \ll u_{10}$. This orthogonal component produces convergent/divergent zones which are aligned with the main flow.

Fig.3 illustrates the expected wind divergence/convergence effects on the development of the waves. The magnitude of the gradient of wind direction G_W is specified here as $|G_W| = 10^{-4}$ rad/m, negative or positive in the divergence or convergence zones, respectively. Small wind direction changes gradually rotate the dominant waves. The divergence of the wind velocity forces the wave rays to widen. In turn, this widening effect results in cross-ray divergence of group velocities, Fig.3, leading to an additional energy sink in the energy balance equation (first term in the r.h.s. in Eq.(42)). For developing waves, this impact is not crucial: an overall energy decrease of about 30%, and subsequent deceleration of the frequency downshift, Fig.3. Ray-divergence effect on the swell is more remarkable, with a rapid attenuation of the energy and shorter peak wavelength away from the wind front, as compared with the reference non-divergent wind, Fig.3.

Figure 3 is about here

Convergent wind field results in more complicated wave development. The wind velocity convergence forces wave rays to progressively concentrate. This inevitably leads to the formation of caustic, where the wave energy locally accumulates. Away from this ray-crossing area, wave-rays widen to become again subject to convergent wind forcing, and the formation of another (new) caustic zone. This process is recurrent, resulting in the modulation of wave energy along the wave development, as well expressed in Fig.3-left. Wave energy modulations cause modulations for the spectral peak frequency, but of second-order in the present case, Fig.3-mid.

If the wind abruptly drops, the impacts of wind forcing on wave direction changes and wave-ray thickening is terminated. In the course of their evolutions, swell trains will then keep memory on the rate of ray thickness widening/narrowing which is constant in time and in space. In the specific case shown in Fig.3, the swell leaves with a decreasing ray width. It then approaches a

caustic zone at distance around $\tilde{x} = 5 \times 10^4$, where the energy largely increases, almost by factor 2 when compared to the reference run. Away from the caustic zone, swell rays diverge, and the energy rapidly attenuates, due to this additional cross-ray divergence of the group velocities.

Application of the 2D parametric model to simulate the surface wave field under stationary and moving cyclones are presented in the companion paper.

6. Summary and Conclusion

A fully consistent 2D parametric model of development of the surface waves parameters (significant wave height, peak frequency and direction) under spatially and temporally varying winds is suggested. The 2D model is based on first-principle conservation equations of the energy and the momentum, consistently constrained by self-similar fetch-laws (15). The model consists of coupled equations written in the characteristic form, which describe development and evolution of wave energy, Eq.(47), group velocity of the spectral peak, Eq.(48), and its direction, Eq.(49). Following the main principle of the parametric model construction, the energy and the group velocity source terms are tuned to reproduce empirical 1D self-similar fetch laws for idealized case of constant wind velocity [Hasselmann et al., 1976].

The wind energy input and wave breaking dissipation are the governing sources of the wave energy evolution. Considering the wind wave growth rate to be $\propto \left(u_* / c\right)^2$, Eq.(3), the wave breaking dissipation becomes a power-function of the dominant wave steepness, Eq.(18). It is suggested that under uniform wind conditions, wave breaking dissipation of developing waves is proportional to the wind energy input. In this case, solution of the energy balance equation (47) in the fetch-law variables (15) exists if exponent q in (15a) is equal to $q = -1/4$. The wave breaking dissipation exponent n in (18) is then linked to the fetch law exponents by relationship (19). The energy source provides growth of the wave energy while waves are young and developing. If wind velocity locally is dropped or/and changes the direction, the wind forcing is

reduced, and the dissipation leads to the energy attenuation, providing smooth transition of wave field from wind driven seas to swell.

Non-linear interactions are essential to drive the spectral peak frequency downshift. In terms of peak group velocity, its growth is proportional to the peak wave steepness to power 4, Eq.(48). Under uniform wind field condition, solution of this equation in fetch-law variables (15) requires fulfilment of the magic relationship (29) between the energy and frequency exponents, as found by Badulin et al. (2007) and Zakharov (2010). Since q is already defined, $q = -1/4$, the fetch exponent for the energy must be $p = 3/4$, conform with Toba [1972]'s relationships. This set of fetch law exponents imposes the power $n = 2$ in the wave breaking dissipation (18).

The non-linear interactions govern the peak frequency downshift as long as the waves are young. When the peak phase velocity approaches wind velocity, the wind energy input to the waves rapidly decays and acts against the downshift driven by non-linear four-wave interactions. Near inverse wave age $\alpha \approx 1$, the magnitudes of non-linear and wind-induced downshift rates are comparable, but with opposite signs. This leads to the leveling off the peak frequency and appearance of so called the "fully-developed" seas.

It is important to emphasize, it is the parametrization of the growth rate in form (3), i.e. as $\propto \left(u_* / c\right)^2$ for uniform wind conditions, which leads to the fetch-laws type solutions (15) with the exponents $q = -1/4$ and $p = 3/4$, that, in turn, also prescribe exponent $n = 2$ in wave breaking dissipation (18). If an alternative parametrization of the growth rate is chosed, e.g. as a linear function of u_* / c, this ultimately leads to another set of the exponents: $q = -1/3$, $p = 7/6$, and $n = 4$. Such fetch-law exponents are also plausible [see e.g. review by Badulin et al., 2007], and may potentially be adopted in the model. However, the present model utilizes the wind wave growth rate in form (3) which was comprehensively grounded either theoretically and experimentally.

Final tuning of the model is to determine proportionality constants in the energy, Eq.(47), and peak group velocity, Eq.(48), evolution equations. These constants are

unambiguously linked with the pre-exponent constants in the fetch-laws (15) (known empirically) with predefined q=-1/4 and p=3/4, and their determination complete the tuning of 2D parametric model.

Under veering wind conditions, neither dissipation nor non-linear interactions are capable to change direction of the spectral peak waves. The wind forcing is the only source to drive wave direction change, and its rate is fully defined by magnitude and the frequency-azimuth dependence of the wind growth rate, i.e. no extra tuning of the model is needed.

Varying winds can then lead to the occurrence of focusing/defocusing wave groups to affect the energy balance. The focusing of wave-rays leads to the possible formation of caustics over areas where wave-rays merge and cross. Formally, the energy balance equation loses its validity with solutions tending to infinity. However, dominant waves in nature have a finite spectral spread and random phases. Caustic locations for the different spectral beams, forming the spectrum of dominant waves, are thus randomly scattered in space. This precludes fully singular behavior, and solutions are found to predict significant (but finite) enhancements of the energy over the focusing caustic zones. Further propagating, wave rays diverge, leading to wave attenuation away from the storm area (Munk et al., 1963, Snodgrass et al., 1966, Ardhuin et al., 2009, Delpey et al., 2010).

Under spatially and time varying winds, this 2D parametric model can thus provide practical means to rapidly map and assess how the energy (significant wave height), frequency and direction of dominant surface waves are distributed. Full sophisticated spectral wave models certainly have these capabilities, as e.g. demonstrated by Moon et al. [2003]. Yet, the proposed simplified 2D parametric model offer very fast wave ray-characteristic solutions, to accommodate for both rapid ensemble evaluations and sensibility studies to model wind adjustments (e.g., Hell et al., 2020). Applications can also serve to provide prior-information to analyze high-resolution satellite remote sensing measurements [e.g. Kudryavtsev et al., 2015, Mouche et al., 2019].

Within the storm generated area, the proposed model also provides relationships to assess the varying breaking distribution of the dominant waves. For intense and varying wind conditions, the distributed thickness of foam layers is then expected to be spatially varying and strongly wave-age dependent. This may have practical applications to improve the interpretation of emitted radiations from thick foam-induced brightness temperatures to low-frequency microwave measurements, especially under extreme conditions (e.g. Reul et al., 2012, Reul et al., 2017).

Further methodological improvements may certainly be foreseen. In particular, the validation of the main features and properties of directional swell systems that outrun their generating strong wind areas can presently benefit from the combined data collected by extensive in situ buoy and remote sensing measurements (e.g. Collard et al., 2009), including the recently launched China-France Ocean Satellite (CFOSAT) SWIM instrument (Hauser et al., 2020) and Copernicus Sentinel-1A and -B SAR measurements. From more systematic comprehensive study of swell fields and the present development, directional peak wave properties may be improved, and possibly more directly parameterized based on the storm structure and intensity, translation and rotation. Such an effort can help improve the physics of numerical wave models and has applications to remote sensing algorithm developments.

Application of the proposed 2D parametric model to simulate the surface wave field under stationary and moving tropical cyclones are presented in the companion paper.

***Acknowledgments*:**

The core support for this work was provided by the Russian Science Foundation through the Project №17-77-30019 at RSHU. The support of the Ministry of Science and Education of the Russian Federation under State Assignment No. 0827-2019-0004 at MHI RAS, and State Assignment No. 0763-2020-0005 at RSHU are gratefully acknowledged.

APPENDIX 1: Effect spectral width on caustic.

Let us assume that the wave field is represented by superposition of elementary monochromatic beams. Elementary waves at a given time t, as well as their contributions to cross-ray divergence, are distributed along the ray around the mean position $l = \overline{c}_g t$ within the interval $\Delta l / l = \pm \Delta c_g / \overline{c}_g$.

To take into account the integrated impact of these wave beams on cross-ray group velocity divergence, the evolution is considered over small space-time scales, much smaller than scales of the wave development. From (4.38), $\Delta\varphi_p = \text{const}$ and the wave beam width varies as $\Delta n = \Delta n_0 + \Delta\varphi_p (l - l_0)$, where $\Delta n_0 = \Delta n(t_0)$, $l_0 = l(t_0)$, and $l = l_0 + c_g (t - t_0)$. Consequently, cross-ray gradient, $G_n = \Delta\varphi_p / \Delta n$, for an elementary beam reads

$$\begin{aligned} G_n &= G_{n0} / \left[1 + G_{n0}(l - l_0)\right] \\ &= 1 / (l - l_c) \end{aligned} \qquad \text{(A1.1)}$$

where $G_{n0} = \Delta\varphi_p / \Delta n_0$, and $l_c = l_0 - 1 / G_{n0}$ is the caustic location for a beam.

For the sake of simplicity, a Gaussian distribution relative to the mean value, $\overline{c}_g$, is considered. Using the JONSWAP spectrum, the standard deviation (std) of this Gaussian distribution can be evaluated. Relative to the carrying wave position, $\overline{l}$, the positions of the elementary waves then obey a Gaussian distribution:

$$P(\delta l) = 1 / \left(\sqrt{\pi}\Delta l\right) \exp\left(-\delta l^2 / \Delta l^2\right) \qquad \text{(A1.2)}$$

where $\delta l = l - \overline{l}$, and Δl is std of positions defined as $\Delta l = \left(\Delta c_g / \overline{c}_g\right) l_c$. The mean value of (A.1) averaged over all wave beams, $\overline{G}_n$, at a point $\overline{l} = \overline{l}(t)$ on the ray is:

$$\begin{aligned} \overline{G}_n(\overline{l}) &= \int_{-\infty}^{+\infty} G_n(l) P(l - \overline{l}) dl \\ G_n(l) &= 1 / \left(l - l_c\right) \end{aligned} \qquad \text{(A1.3)}$$

Fig. A-1 shows estimated mean cross-ray gradients of ray directions. Taking into account the finite spectral width of the wave groups removes asymptotic singularities for the energy focusing in the vicinity of a caustic point.

In practice, integral (A.3) can be approximated by the expression

$$G_n/G_{n0} = \frac{l/l_c - 1}{\left(l/l_c - 1\right)^2 + \left(1/2 \cdot \Delta c_g/c_g\right)^2} = \frac{\Delta n/\Delta n_0}{\left(\Delta n/\Delta n_0\right)^2 + \left(1/2 \cdot \Delta c_g/c_g\right)^2} \tag{A1.4}$$

A modified expression for the cross-ray gradient of ray directions, uniformly valid everywhere including caustic zones, can thus be suggested

$$G_n = \frac{\Delta\varphi_p}{\Delta n_0}\left[\frac{\Delta n/\Delta n_0}{\left(\Delta n/\Delta n_0\right)^2 + \left(1/2 \cdot \Delta c_g/\overline{c}_g\right)^2}\right] \tag{A1.5}$$

where $\Delta\varphi_p$ and Δn are solutions of equations (4.41) and (4.38), correspondingly, with $\Delta c_g/\overline{c}_g$ the group velocity std scaled by the mean value.

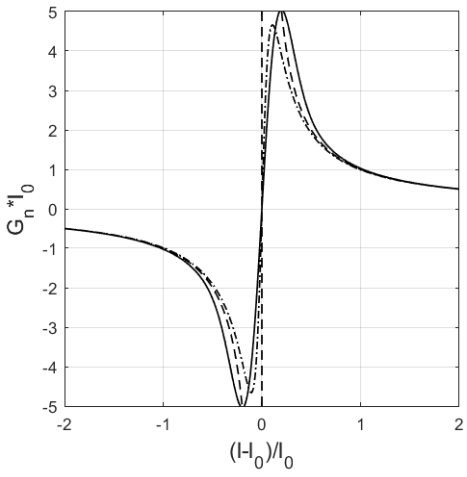

Figure A-1. Cross-ray gradient of wave directions around the caustic point for: (dash line) monochromatic wave, solution of (43); (solid line) wave packet with Gaussian distribution of group velocities, relation (A.1.3); (dash-dotted) approximate relation (A.1.5).

APPENDIX 2: Choice of model constants

In this section we justify and summarize the constants which involved in the model construction.

The growth rate constant, c_β, in (3b) varies in the range $c_\beta = (2 \div 6) \times 10^{-2}$ [Plant, 1982]. In the model it is fixed at $c_\beta = 4 \times 10^{-2}$. In the range from moderate to high winds, the surface drag coefficient, c_D, is described by empirical relationships. There are much more uncertainties for c_D at high winds, above 20m/s, and a conventional agreement is to consider c_D to saturate around $c_D = 2 \times 10^{-3}$. Targeting simulation of the waves under TC, we adopt this value in our model.

The fetch low exponents p and q in (15a) are already prescribed in the model as $p = 3/4$, and $q = -1/4$. To specify other fetch-low constants c_α and c_e, we follow critical overview by Badulin et al. [2007]. Among number of empirical fetch-laws, the relationship suggested by Babanin and Soloviev [1998] was singled out as the most preferable, because it satisfies to the magic relation between fetch-law exponents. Since this magic relation plays the key role in our model, we choose Babanin and Soloviev [1998] parametrization as a reference empirical data. The model exponents q and p are slightly different from that reported by Babanin and Soloviev (1998): q = - 0.275, p/q = -3.01. To get the best fit with Babanin and Soloviev [1998] reported data, we specify c_α and c_e in our model as:

$$c_\alpha = 11.8 \text{ and } c_e = 1.3 \times 10^{-6}. \qquad \text{(A2.1)}$$

Correspondingly, the dissipation exponent n is

$$n = \frac{2q}{p + 4q} = 2 \qquad \text{(A2.2)}$$

At fixed $c_\beta = 4 \times 10^{-2}$ and $c_D = 2 \times 10^{-3}$, the dimensionless factor “wind-input-minus-dissipation”, $(1 - \gamma)$, becomes

$$(1 - \gamma) = (p - q) c_\alpha^{-4} / (2 r c_\beta c_D) = 0.12, \qquad \text{(A2.3)}$$

Accordingly $\gamma = 0.88$, and the threshold steepness in dissipation is

$$\varepsilon_T^2 = \frac{c_e c_\alpha^{-p/q}}{\left(\gamma c_\beta c_D\right)^{1/n}} = 0.15 \qquad \text{(A2.4)}$$

Remarkably, if we express ε_T^2 via steepness $\varepsilon_T^2 = a^2k^2/2$, this value appears consistent with the vertical acceleration at the crest approaching $-g/2$ and a limiting Stokes-wave steepness, ak, equal to 0.5.

Finally, the model constants for the energy and the peak frequency evolutions, are defined as

$$C_e = 1/2 \times \left[(p-q)/(1-\gamma)\right] c_\alpha^{-4} = 2.16 \times 10^{-4} \qquad \text{(A2.5)}$$

$$C_\alpha = 1/2 \times q c_\alpha^{-10} c_e^{-2} = -1.4 \qquad \text{(A2.6)}$$

Constant C_φ, necessary for the evolution of the spectral peak direction, is evaluated with an angular spreading $\delta\varphi^2 = 0.16$ (typical for JONSWAP spectrum) and the integral spectral bandwidth taken in the range $\bar{\omega} - \delta\omega < \omega < \bar{\omega} + \delta\omega$ ($\delta\omega$ is the standard deviation of JONSWAP spectrum frequency spreading), to give

$$C_\varphi = c_\beta c_D \delta\varphi^2 \frac{\int \omega^4 F(\omega) d\omega}{\omega_p^3 \int \omega F(\omega) d\omega} = 1.8 \times 10^{-5} \qquad \text{(A2.7)}$$

All the model constants are summarized in the table below.

TABLE 1: SUMMARY OF THE MODEL CONSTANTS

Constant	Value	Number of equation (where it appears)	Comment
c_D	2e-3	13b	Drag coefficient
c_β	4e-2	11b	Growth rate constant
p	¾	15a,b	Fetch low exponent for energy
q	-1/4	15a,b, 22	Fetch low exponent for frequency
c_α	11.8	15a,b	Fetch-low constant for frequency
c_e	1.3e-6	15a,b	Fetch-low constant for energy

n	2	18	Exponent for wave breaking dissipation
ε_T^2	0.15	18, 25	Threshold steepness for wave breaking dissipation
$\delta\varphi^2$	0.16	13b	Angular spread of wave energy
γ	0.88	20, 24	Dissipation over wind input ratio, D/I_w
r_g	0.87	8, 17, 20, 24, 25	$\overline{c}_g/c_{gp}, \omega_p/\overline{\omega}$
r_w	2.35	17, 20, 24, 25, 48	$\int \omega^3 F d\omega/(\omega_p{}^3 e)$
C_e	2.16e-4	26	Constant in energy evolution equation
C_a	-1.41	31, 48	Constant in group velocity evolution equation
C_φ	1.8e-5	13b, 49	Constant in peak direction evolution equation

References

Ardhuin, F., Chapron, B., and F. Collard, (2009), Observation of swell dissipation across oceans, *Geophys. Res. Lett., 36*, L06607, doi:10.1029/2008GL037030.

Babanin, A. N., and Y. P. Soloviev, (1998), Field investigation of transformation of the wind wave frequency spectrum with fetch and the stage of development, *J. Phys. Oceanogr. 28*, 563–576.

Badulin S. I., A. V. Babanin, V. E. Zakharov, and D. Resio (2007), Weakly turbulent laws of wind-wave growth, *J. Fluid Mech., 591*, 339–378, doi:10.1017/S0022112007008282.

Badulin S. I., and V. E. Zakharov, (2017), Ocean swell within the kinetic equation for water waves, *Nonlin. Processes Geophys., 24*, 237–253, doi: 10.5194/npg-24-237-2017

Bowyer, P. J., and A. W. MacAfee (2005), The theory of trapped-fetch waves with tropical cyclones - An operational perspective, *Weather Forecasting, 20,* 229–244, doi:10.1175/WAF849.1.

Brumer, S. E., Zappa, C. J., Brooks, I. M., Tamura, H., Brown, S. M., Blomquist, B. W., and A. Cifuentes-Lorenzen (2017), Whitecap coverage dependence on wind and wave statistics as observed during SO GasEx and HiWinGS, *J. Phys. Oceanogr., 47(9)*, 2211-2235.

Collard, F., F. Ardhuin, and B. Chapron (2009), Monitoring and analysis of ocean swell fields from space: New methods for routine observations, *J. Geophys. Res., 114*, C07023, doi:10.1029/2008JC005215.

Delpey, M. T., Ardhuin, F., Collard, F., and B. Chapron (2010), Space-time structure of long ocean swell fields, *J. Geophys. Res., 115*, C12037, doi:10.1029/2009JC005885.

Dysthe, K. B., and A. Harbitz (1987), Big waves from polar lows?, *Tellus, Ser. A, 39*, 500–508, doi:10.1111/j.1600-0870.1987.tb00324.x.

Fontaine, E. (2013), A Theoretical Explanation of the Fetch- and Duration-Limited Laws, *J. Phys. Oceanogr. 43 (2)*, 233-247, DOI: 10.1175/JPO-D-11-0190.1

Hasselmann, K., D. B. Ross, P. Müller, and W. Sell (1976), A Parametric Wave Prediction Model, *J. Phys. Oceanogr., 6,* 200-228, doi:10.1175/1520-0485(1976)006<0200: APWPM>2.0.CO;2.

Hasselmann, K. (1974). On the spectral dissipation of ocean waves due to whire-capping. *Boundary Layer Meteor., 6*, 107-127

Hasselmann, D. E., Rosenthal and M. Dunckel (1980), Directional wave spectra observed during JONSWAP 1973, *J. Phys. Oceanogr., 10*, 1264-1280

Hasselmann, K., (1962). On the nonlinear energy transfer in a gravity-wave spectrum. Part 1. General theory, *J. Fluid Mech., 12*, 481–500.

Hasselmann, S., Hasselmann, K., Allender, J. H.m and T.P. Barnett (1985), Computations and parametrizations of the nonlinear energy transfer in a gravity-wave spectrum. Part II. Parameterizations of the nonlinear energy transfer for application in wave models. *J. Phys. Oceanogr. 15,* 1378–1391

Hauser D., Tourain C., Hermozo L., Alraddawi D., Aouf L., Chapron B., Dalphinet A., Delaye L., Dalila M., Dormy E., Gouillon F. et al. (2020), New observations from the SWIM radar on board CFOSAT: instrument validation and ocean wave measurement assessment, *IEEE Transactions on Geoscience and Remote Sensing*, DOI: 10.1109/TGRS.2020.2994372

Hell, M. C., B. D. Cornuelle, S. T. Gille, A. J. Miller, and P. D. Bromirski (2019), Identifying ocean swell generation events from Ross Ice Shelf seismic data, *J. Atmos. Oceanic Technol.,* DOI:10.1175/JTECH-D-19-0093.1

Hwang P., and E. Walsh (2018), Propagation Directions of Ocean Surface Waves inside Tropical Cyclones, *J. Phys. Oceanogr., 48 (7),* 1495-1511, DOI:10.1175/JPO-D-18-0015.1.

Hwang P, and Y. Fan (2017), Effective fetch and duration of tropical cyclone wind fields estimated from simultaneous wind and wave measurements: Surface wave and air–sea exchange computation, *J. Phys. Oceanogr., 47*, 447–470, DOI:10.1175/JPO-D-16-0180.1.

Gunther H., W. Rosenthal, T. J. Weare, B. A. Worthington, K. Hasselmann, and J. A. Ewing (1979), A hybrid parametrical wave prediction model, *J. Geoph. Res., 84, C9*, DOI:10.1029/ jc084ic09p05727

Gunther H., W. Rosenthal and M. Dunckel (1981), The response of surface gravity waves to changing wind direction, *J. Phys. Oceanogr., 11*, 718-728

King, D. B., and O. H. Shemdin (1978), Radar observations of hurricane wave directions, in *Proceedings of 16th International Conference on Coastal Engineering*, pp. 209–226, Am. Soc. of Civ. Eng., Hamburg, Germany.

Kitaigorodskii, S.A. (1962), Applications of the theory of similarity to the analysis of wind-generated water waves as a stochastic process, *Bull. Acad. Sci. USSR Geophys. Ser., 1*, 105–117.

Kudryavtsev, V., P. Golubkin, and B. Chapron (2015), A simplified wave enhancement criterion for moving extreme events, *J. Geophys. Res. Oceans, 120,* 7538-7558, doi:10.1002/2015JC011284

Longuet-Higgins M. S. (1969), On wave breaking and the equilibrium spectrum of wind generated waves. *Proc. Roy. Soc., A310,* 1501, l5l-159.

Meirink, J.F., Kudryavtsev, V.N. and V.K. Makin (2003), Note on the growth rate of water waves propagating at an arbitrary angle to the wind, *Boundary-Layer Meteorol, 106*, 171-183.

Moon, I.-J., I. Ginis, T. Hara, H. L. Tolman, C. W. Wright, and E. J. Walsh (2003), Numerical simulation of sea surface directional wave spectra under hurricane wind forcing, *J. Phys. Oceanogr., 33*, 1680–1706, doi:10.1175/2410.1.

Mouche, A., Chapron, B., Knaff, J., Zhao, Y., Zhang, B., and C. Combot (2019). Copolarized and cross-polarized SAR measurements for high-resolution description of major hurricane wind structures: Application to Irma category 5 hurricane. *J. Geoph. Res.: Oceans, 124*, 3905– 3922. DOI:10.1029/2019JC015056

Munk, W. H., G. R. Miller, F. E. Snodgrass, and N. F. Barber (1963), Directional recording of swell from distant storms, *Philos. Trans. R. Soc. London, Ser. A, 255*, 505–584.

Plant, W. J. (1982), A relation between wind stress and wave slope, *J. Geoph. Res., 87*, 1961-1067

Phillips, O. M. (1985), Spectral and statistical properties of the equilibrium range in the wind-generated gravity waves, *J. Fluid Mech., 156*, 505 –531

Phillips, O. M., (1977). The Dynamics of the Upper Ocean, 366 pp., Cambridge Univ. Press, New York, 1977.

Pushkarev A., and V. Zakharov (2015), On nonlinearity implications and wind forcing in Hasselmann equation. *arXiv:1503.07091* [physics.ao-ph]

Reul, N., and B. Chapron (2003), A model of sea-foam thickness distribution for passive microwave remote sensing applications, *J. Geophys. Res., 108, C10,* 3321, DOI:10.1029/2003JC001887.

Reul, N., Tenerelli, J., Chapron, B., Vandemark, D., Quilfen, Y., and Y. Kerr (2012), SMOS satellite L-band radiometer: A new capability for ocean surface remote sensing in hurricanes, *J. Geophys. Res., 117, C02006*, doi:10.1029/2011JC007474.

Reul, N., B. Chapron; E. Zabolotskikh; C. Donlon; A. Mouche; J. Tenerelli; F. Collard; J. F. Piolle; A. Fore; S. Yueh J. Cotton; P. Francis; Y. Quilfen; V. Kudryavtsev (2017), A New Generation of Tropical Cyclone Size Measurements from Space, *Bull. Amer. Meteor. Soc., 98*, 2367–2385, DOI:10.1175/BAMS-D-15-00291.1.

Snodgrass, F. E., G. W. Groves, K. Hasselmann, G. R. Miller, W. H. Munk, and W. H. Powers (1966), Propagation of ocean swell across the Pacific, *Philos. Trans. R. Soc. London, Ser. A, 249*, 431–497.

Snyder, R., F. Dobson, J. Elliott, and R. Long (1981), Array measurement of atmospheric pressure fluctuations above surface gravity waves, *J. Fluid Mech., 102*, 1–59.

Toba, Y., (1972), Local balance in the air-sea boundary processes. *Journal of the Oceanographical Society of Japan, 28,* 109–120, DOI:10.1007/BF02109772

Tolman, H. L. (2004), Inverse modeling of discrete interaction approximations for nonlinear interactions in wind waves, *Ocean Model., 6,* 405–422.

Tolman, H. L. (2009), User manual and system documentation of WAVEWATCH III version 3.14, Tech. Note 276, 194 pp., NOAA/NWS/NCEP/MMAB, Camp Springs, Md.

Tulin M. (1996), Breaking of ocean waves and downshifting. *Waves and Nonlinear Processes in Hydrodynamics, J. Grue, B. Gjevik, and J. E. Weber, Eds*., Kluwer Academic Pubishers, 177–190.

van Vledder G., P, and L.H. Holthuijsen (1993), The directional Response of Ocean Waves to Tuning Winds, *J. Phys. Oceanogr., 23,* 718-728.

Young, I. R. (1988), A parametric hurricane wave prediction model, *J. Waterw. Port Coastal Ocean Eng., 114(5),* 637–652, doi:10.1061/(ASCE)0733-950X(1988)114:5(637).

Young, I. R., and J. Vinoth (2013), An ‘‘extended fetch’’ model for the spatial distribution of tropical cyclone wind-waves as observed by altimeter, *Ocean Eng., 70,* 14–24, doi:10.1016/j.oceaneng.2013.05.015.

Wright, C.W., E.J. Walsh, D. Vandemark, W.B. Krabill, A.W. Garcia, S.H. Houston, M.D. Powell, P.G. Black, and F.D. Marks (2001), Hurricane directional wave spectrum spatial variation in the open ocean. *J. Phys. Oceanogr., 31,* 2472–2488.

Zakharov, V.E. (2010), Energy balances in a wind-driven sea, *Physica Scripta, 2010, T142,* 014052.

Figures and Captions

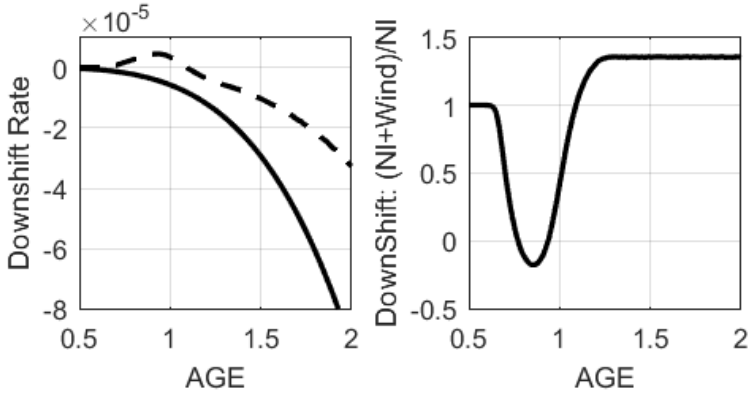

Figure 1. Left plot: solid line is non-linear downshift according to (31), and dash line is down/up-shift due to wind forcing predicted by (32). Right plot: ratio of consolidate shift (non-linear plus wind) to non-linear downshift.

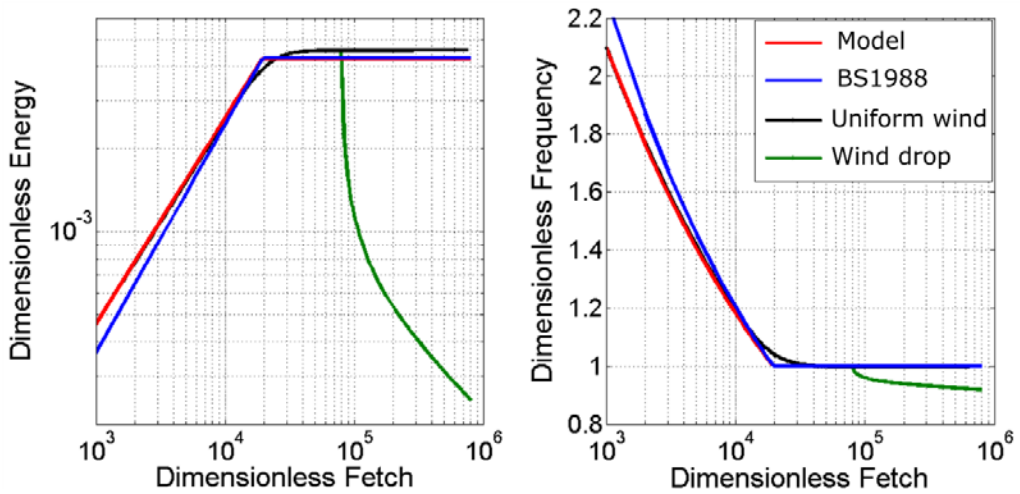

Figure 2. (left) dimensionless energy and (right) peak frequency vs dimensionless fetch. Line notations is given in legend. Green line show model evolution of energy and frequency after the wind suddenly drop at fetch $\tilde{x} = 8 \times 10^4$.

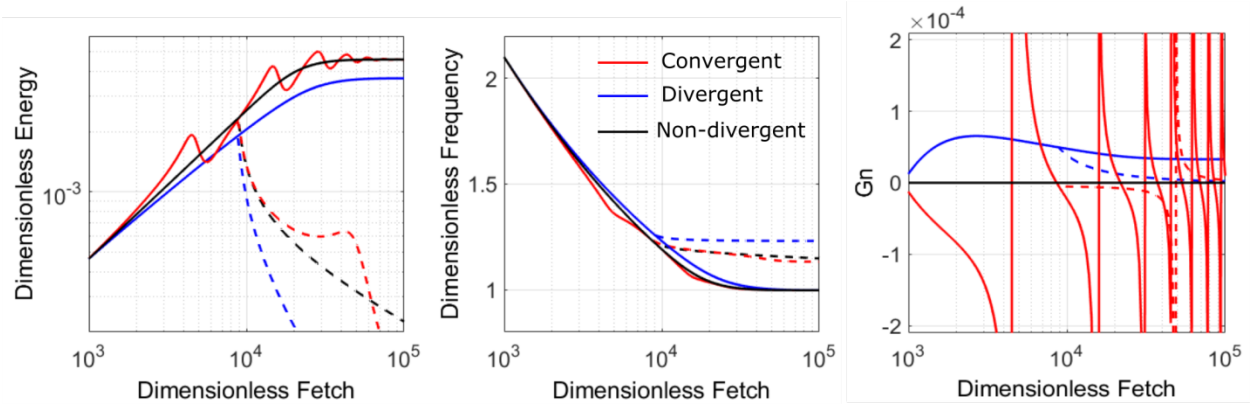

Figure 3. Fetch-limited development of wind wave parameters for (black lines) non-divergent, (blue lines) divergent, and (red lines) convergent off-shore wind field. Dash lines of different colors show model parameters for the case when wind speed is "abruptly vanished: at dimensionless fetch $\tilde{x} = 0.9 \times 10^4$, and the solid lines show the case when wind filed is continuous. Wave parameters are: (left plot) dimensionless energy, (mid plot) dimensionless peak frequency, (right plot) cross-ray gradient of wave directions, Eq.(46).